Fontan Computational Hemodynamics: Impact of Inlet Velocity Profile Features with Implications on Clinically Relevant Parameters

Fontan Computational Hemodynamics: Impact of Inlet Velocity Profile Features with Implications on Clinically Relevant Parameters

M. Lodi Rizzini[1], P. Tasso[1], D. Gallo[1], G. D'Avenio[2], A Secinaro[3], A. Amodeo[3], U. Morbiducci[1] and M. Grigioni[2]
[1] *PolitoBio^{MED}Lab, Department of Mechanical and Aerospace Engineering, Politecnico di Torino, Turin, Italy*
[2] *Istituto Superiore di Sanità, Department of Technology and Health, Rome, Italy*
[3] *Ospedale Pediatrico Bambino Gesù, Department of Pediatric Cardiology and Cardiac Surgery, Rome, Italy*

***Abstract* — Total cavopulmonary connection (TCPC) is a surgical technique adopted for univentricular heart disease treatment. Due to a not physiological postoperative shape of the connection some complications can occur due to thrombus formation and energy dissipation. In this perspective the aim of our study was to analyse the influence of inlets velocity profiles on the local hemodynamic. The results showed that an increase of the helical structures, increase the average value of WSS and reduce the hydraulic energy losses. The final remarks are: (1) only through-plane velocity overestimated the energy dissipation and (2) in-plane velocity could be useful in reducing thrombus formation risk and could increase connection efficiency.**

***Keywords*—Fontan, Thrombus risk, Viscous Dissipation Rate**

I. Introduction

UNIVENTRICULAR heart is a congenital disease with an incidence of about 2% in peadiatric patients with heart diseases [1]. This pathological condition consists in the presence of a single ventricle chamber, with the ultimate consequence of oxygenated and deoxygenated blood mixing [1]. Main complications for this pathology are low blood saturation, chronic cyanosis, and heart failure as a result of volumetric overload. If untreated, this pathological state leads to patients death before 16 years old in the 70% of cases [1]. The most common surgical technique adopted to treat these patients is the Fontan procedure [2]. This surgical techniques consists of three consecutive steps to gradually separate systemic and pulmonary circulations through a connection between the two venae cava and pulmonary arteries [2]. The Fontan procedure is palliative and present complication risks, the most relevant being systemic and pulmonary thrombus formation [3] and an inadequate connection efficiency [4]. These risks are clearly related to the complex venous hemodynamics [3], which could lead to connection failure [5].

In recent years, the coupling of medical imaging and computational fluid dynamics (CFD) has been extensively developed and applied to study cardiovascular flows, taking advantage of the possibility given by CFD to obtain highly resolved hemodynamics in anatomically realistic arterial models. In this sense, CFD have been a powerful instrument to assess Fontan hemodynamics, both in relation to surgical planning and/or optimization [6] and to long-term complications [7]. In the context of a subject-specific oriented approach, 4D flow MRI has emerged as able to provide the anatomical and hemodynamic inputs to even more realistic, fully personalized Fontan flow simulations. The importance of adopting realistic inflow BCs was recently highlighted in cardiovascular flows [8], and very recently investigated also in TCPC models [9].

Motivated from these evidences, the aim of this work was to explore the hemodynamics in a patient-specific 3D model of TCPC with CFD simulations, focusing on the impact of inflow velocity profile features on TCPC hemodynamics, with a tightly controlled approach. To do that, different velocity profiles were analytically generated and prescribed at the inlets (i.e., the superior and inferior cava vein). The impact of the inflow velocity profiles features was evaluated in terms of: (1) thrombus formation risk considering low wall shear stress as an indicator of low/recirculating flow (which is an hallmark of thrombogenicity), (2) intravascular flow features, assessing helical and vortical flow features, and (3) connection efficiency, in terms of hydraulic power losses and viscous dissipation rate.

II. Materials and Methods

A. Fluid Dynamic Simulation and Boundary Conditions

In a patient-specific 3D model of a cavopulmonary connection, the governing equations of fluid motion, the Navier-Stokes equations, were solved in their discretized form under unsteady-state conditions, adopting the finite element-based open-source code SimVascular (http://simvascular.github.io/). To ensure a grid-independence solution of the flow field an average element size of $0.675 \cdot 10^{-3}$ m with a near-wall refinement consisting of 3 tetrahedral boundary layers with a decreasing ratio of 0.6 was adopted after a sensitivity analysis. The resulting mesh cardinality was of 3.5 million elements. Blood was assumed to be an homogeneous, incompressible, Newtonian fluid with density ρ = 1060 kg/m^3 and dynamic viscosity μ = 0.004 Pa·s [10]. Vessels wall was assumed to be rigid, and a no-slip condition was prescribed at wall boundaries. Concerning the outflow sections, hydraulic resistance values based on data proposed in the literature [11] were imposed at the left pulmonary artery (LPA) and at the two right pulmonary arteries (RPA1 and RPA2, respectively), as depicted in Fig. 1. In detail, the value of $2.76\ 10^7\ kg/m^4s$ was imposed as hydraulic resistance at LPA outflow section (R_{LPA}) and as total resistance at the two RPA outflow sections. Then, the resistance values at the two right pulmonary arteries

were set according to the Murray's law [12], obtaining the following hydraulic resistance values: $R_{RPA1} = 5.70\ 10^7\ kg/m^4s$ and $R_{RPA2} = 5.35\ 10^7\ kg/m^4s$. At the inflow sections at the superior and inferior vena cava (SVC and IVC, respectively), Dirichlet boundary conditions were imposed in terms of 3D velocity profiles as detailed in the following section.

B. *Inflow Velocity Profiles*

The 3D velocity profiles at the SVC and IVC inflow sections were built up as given by the combination of two components: a through-plane (TP) component, in the direction of the axis of the vessel and thus orthogonal to the inflow section, and an in-plane (IP) component, orthogonal to the direction of axis of the vessel and this lying on inflow section plane. Due to the lack of patient-specific hemodynamic data, here we used the venous flow rate waveforms of another patient, rescaled to the inlet SVC and IVC areas. Using inflow rate waveforms, the Womersley theory [13] was applied to obtain the instantaneous local TP velocity components at SVC and IVC inlet sections. The presence of the IP component as part of the inflow velocity profile was modelled assuming that two possible main configurations could be representative of the venous secondary flow in the caval veins. More in detail, we considered the presence of (1) one single vortex structure, and (2) Dean-like two-vortex configuration. To generate the secondary flow structures, here two analytical formulations were used, generalized to fit realistic non-circular cross-sections of blood vessels. In detail, starting from the polar coordinate system (r, ϑ) defined on the inlet surface, we defined a new generalized polar coordinate system (r', ϑ'):

$$\begin{cases} r' = \frac{r}{R(\vartheta)} \\ \vartheta' = \vartheta \end{cases} \quad (1)$$

where R(ϑ) is the variable radius of inlet surface. This allow to have values of r' ranging from 0 to 1 (0 at the surface geometric centre and 1 at each point of surface boundary).
The first formulation, describing one single vortex secondary flow configuration (Fig. 1), was obtained generalizing the equation proposed elsewhere [14], as follows:

$$\begin{cases} \boldsymbol{v}_{\vartheta'}(r', \vartheta') = k_{\vartheta'}[1 - r'^2]r'\boldsymbol{u}_{\vartheta'} \\ \boldsymbol{v}_{r'}(r', \vartheta') = k_{r'}[1 - r'^2]r'\boldsymbol{u}_{r'} \end{cases} \quad (2)$$

where $\boldsymbol{u}_{r'}$ and $\boldsymbol{u}_{\vartheta}$ are unit vectors along the radial and angular direction respectively, and $k_{\vartheta'}$ and $k_{r'}$ are constant parameters regulating the angular and radial component of IP velocity, respectively. In this study the values $k_{\vartheta'}$=5 and $k_{r'}$=1 were considered to obtain the single-vortex secondary flow configuration. The second formulation describes a double-vortex secondary flow configuration, obtained generalizing to non-circular cross-sections the Dean formulation for secondary flows in curved pipes [15]:

$$\begin{cases} \boldsymbol{v}_{\vartheta'}(r', \vartheta) = (1 - r'^2)(4 - 23r'^2 + 7r'^4)\cos(\vartheta')\,\boldsymbol{u}_{\vartheta'} \\ \boldsymbol{v}_{r'}(r', \vartheta) = (1 - r'^2)^2(4 - r'^2)\sin(\vartheta')\,\boldsymbol{u}_{r'} \end{cases} \quad (3)$$

On both the SVC and IVC inlet section, the local value of the IP component of the inflow velocity was then scaled to the instantaneous inflow rate waveform according to:

$$\boldsymbol{v}_{ip}(r', \vartheta', t) = C\frac{Q(t)}{S}\frac{\boldsymbol{v}_{\vartheta'}(r', \vartheta') + \boldsymbol{v}_{r'}(r', \vartheta')}{|\boldsymbol{v}_{\vartheta'}(r', \vartheta') + \boldsymbol{v}_{r'}(r', \vartheta')|_{mean}} \quad (4)$$

where Q(t) is time-dependent inlet flow rate, S is the inlet surface area and C is the scaling factor. Here two values were set for the parameter C, i.e., C=0.33 and C=0.66, corresponding to a magnitude ratio of the local IP and TP velocity components equal to 33% and 66%, respectively. Summarizing, five unsteady-state simulations were performed on the same TCPC model with different velocity profiles as inflow boundary condition (TABLE I): the one-dimensional, only TP Womersley velocity profile was used as reference case, and four three-dimensional profiles made by the composition of Womersley profile as TP component and different IP components.

TABLE I

Profile Name	*TP velocity*	*IP velocity*	*IP/TP*
Reference	Womersley	No IP velocity	0.00
Double Vortex IP33	Womersley	Double Vortex	0.33
Double Vortex IP66	Womersley	Double Vortex	0.66
Single Vortex IP33	Womersley	Single Vortex	0.33
Single Vortex IP66	Womersley	Single Vortex	0.66

Schematic table of the different velocity profiles adopted in the study

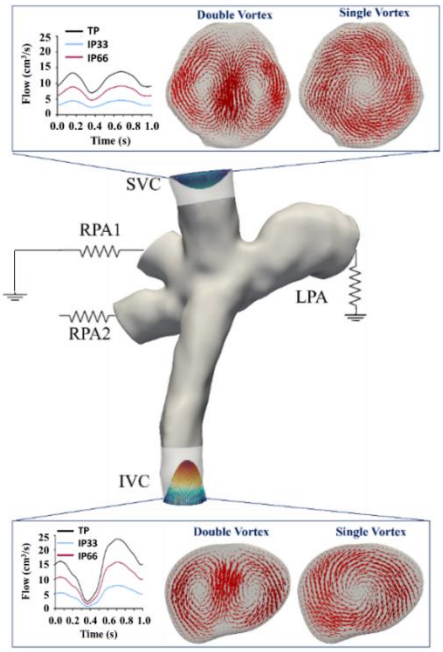

Fig. 1: Schematic of BCs applied at inflow and outflow sections of the TCPC model. In upper and lower panels details about inflow BCs, at SVC and IVC respectively are reported: on the left the time dependant flowrate of TP and scaled amount of IP; in the middle and on the right the IP velocity scaled vectors for double and single vortex configurations respectively.

C. *Hemodynamic Descriptors*

The near-wall hemodynamics was characterized in terms of time-averaged wall shear stress (TAWSS), as indicator of low velocity/ stagnation regions, computed as:

$$\mathrm{TAWSS}(s) = \frac{1}{T}\int_0^T |\boldsymbol{\tau}_w(\boldsymbol{s}, t)|\,dt \quad (5)$$

where T is the time duration of the cardiac cycle, $\boldsymbol{\tau}_w$ the wall shear stress vector, and $\boldsymbol{s}$ the position at the wall. Moreover, the intravascular flow features were analysed in terms of helical flow and vorticity. In particular, to visualize helical flow patterns, the local normalized helicity (LNH) was computed as follows [16]:

$$\mathrm{LNH} = \frac{\boldsymbol{v}(s,t)\cdot\boldsymbol{\omega}(s,t)}{|\boldsymbol{v}(s,t)\cdot\boldsymbol{\omega}(s,t)|} = \cos\varphi \quad (6)$$

where φ is the angle between the velocity ($\boldsymbol{v}$) and vorticity ($\boldsymbol{\omega}$) vector. The analysis was completed evaluating the efficiency of the TCPC in terms of hydraulic power and energy dissipation. In detail, the instantaneous hydraulic power losses ($\dot{E}$) [17] was evaluated as follows:

$$\dot{E}(t) = -\int_{IN} p(\boldsymbol{s},t)\boldsymbol{v}(\boldsymbol{s},t)\cdot\boldsymbol{u}_n(\boldsymbol{s})dS - \int_{IN}\frac{1}{2}\rho|\boldsymbol{v}(\boldsymbol{s},t)|^2\boldsymbol{v}(\boldsymbol{s},t)\cdot\boldsymbol{u}_n(\boldsymbol{s})dS - \int_{OUT} p(\boldsymbol{s},t)\boldsymbol{v}(\boldsymbol{s},t)\cdot\boldsymbol{u}_n(\boldsymbol{s})dS - \int_{OUT}\frac{1}{2}\rho|\boldsymbol{v}(\boldsymbol{s},t)|^2\boldsymbol{v}(\boldsymbol{s},t)\cdot\boldsymbol{u}_n(\boldsymbol{s})dS \quad (7)$$

where p is the pressure and $\boldsymbol{u}_n$ the outward unit vector normal to inlet/outlet sections. The local viscous dissipation rate (VDR) [9] in the TCPC fluid domain was evaluated according to:

$$\mathrm{VDR}(\boldsymbol{s},t) = \mu\left[2\left(\frac{\partial v_x}{\partial x}\right)^2 + 2\left(\frac{\partial v_y}{\partial y}\right)^2 + 2\left(\frac{\partial v_z}{\partial z}\right)^2 + \left(\frac{\partial v_x}{\partial y}+\frac{\partial v_y}{\partial x}\right)^2 + \left(\frac{\partial v_x}{\partial z}+\frac{\partial v_z}{\partial x}\right)^2 + \left(\frac{\partial v_y}{\partial z}+\frac{\partial v_z}{\partial y}\right)^2\right] \quad (8)$$

where v_x, v_y and v_z are the three velocity components in the cartesian coordinate system. The TCPC was characterized in terms total VDR in the whole TCPC fluid volume V:

$$\mathrm{VDR}_{tot}(t) = \int_V \mathrm{VDR}(\boldsymbol{s},t)dV \quad (9)$$

III. Results

The surface areas at the luminal surface subjected to TAWSS values lower than 0.4 Pa are presented in Fig. 2. From a qualitative point of view, it can be noticed that, especially in the graft area, TAWSS values are higher if an IP velocity component is prescribed at the inflow sections. The quantitative evaluation of the surface exposed to low WSS (Fig. 2), confirm the previous observation, where it can be noticed that the imposition of a purely TP velocity profile at the inflow sections leads to a larger luminal surface exposed to low TAWSS.

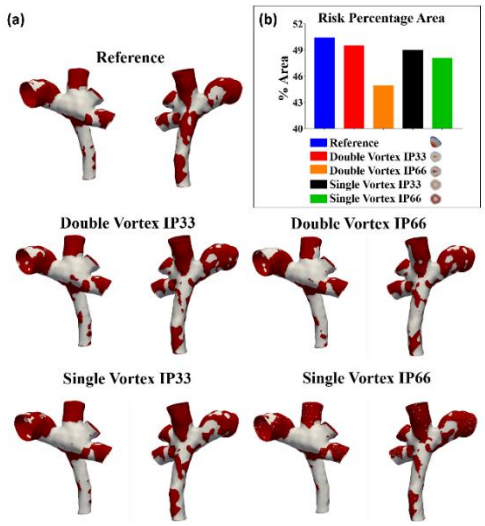

Fig. 2: (a) 3D model surfaces areas subjected to TAWSS < 0.4 Pa and (b) percentage histogram of surface subjected to low WSS.

A picture of the helical flow patterns inside the TCPC is presented in Fig. 3 in terms of isosurfaces of LNH (averaged over the cardiac cycle). By visual inspection of Fig. 3, it emerges that the cases with 3D velocity profiles as inflow BCs present a larger counter-rotating helical patterns, with respect to the reference only TP inflow BC velocity profiles.

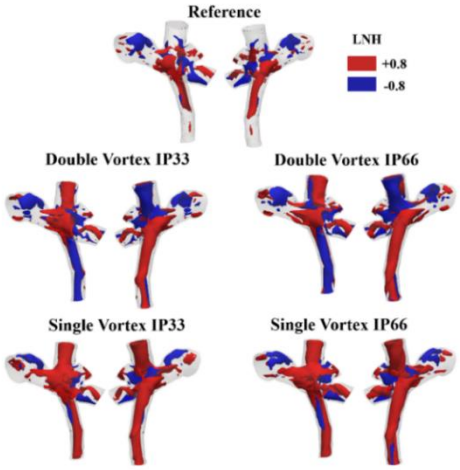

Fig. 3: LNH iso-surfaces for the five velocity profiles imposed, thresholds was set at ±0.8 for visualization purposes. righthanded and lefthanded structures are coloured in red and blue respectively.

Finally, differences in energy dissipation rate distribution within the TCPC, depending on inflow BC velocity profiles can be observed in Fig. 4 in terms of streamlines of the cycle-average flow field (colour-coloured with VDR values). It can be noticed that the only TP inflow BC case presents high VDR values (particularly in the anastomosis region).

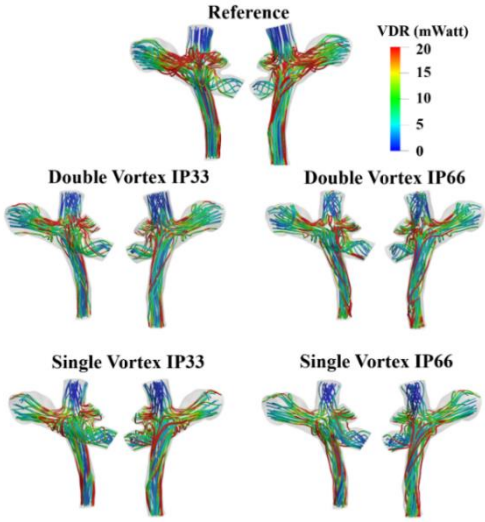

Fig. 4: colormaps of streamlines according to VDR for the five velocity profiles imposed.

These qualitative observations are also confirmed by the quantitative analysis in Fig. 5. All 3D inflow velocity profile BCs cases are characterized by power loss cycle-average values of power losses and VDR_{tot} lower that than only TP case, except for the case double vortex IP66. Finally, it was observed that TCPC power losses are sensitive to the shape on the inflow velocity profiles. In detail, the case corresponding to only TP velocity profile as inflow BCs presented cycle-average power loss value markedly higher (Fig. 5) than the cases with 3D inflow velocity profiles.

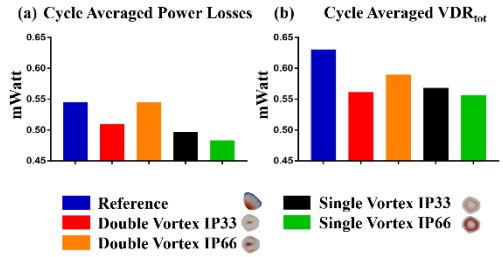

Fig. 5: histograms of time average values of (a) power losses and (b) viscous dissipation rate for the five different velocity profiles imposed.

IV. Discussions and Conclusion

TCPC surgical intervention, in consequence of its not physiological reshaping of the circulation, does not guarantee a long-term stability [4]. In fact, it is well established that, the TCPC local hemodynamic plays a key role in the long-term outcome [4], [9]. In this context, due to its high spatial and temporal resolution, CFD is a powerful tool to investigate the patient-specific hemodynamics. The importance of realistic inflow boundary conditions in cardiovascular flow simulations was recently established [8] and very recently studied also in TCPC models [9]. Due to the impact that assumption/idealization have in personalized in silico hemodynamics, in this study we investigated if the shape of the venous velocity profiles applied as inflow condition at SVC and IVC inlet sections of TCPC computational hemodynamics models has some impact in the hemodynamics of the anastomosis region, with particular attention to thrombus formation, hydraulic power and energy dissipation, clinical hallmarks of TCPC failure.

To do that, TP and IP analytical, generalized velocity profiles were assembled, based on fluid mechanics theory and CFD simulations were carried out on a TCPC model.

The findings of this study suggest that the presence of the IP component in the velocity profile prescribed as venous inflow BC, compared to a purely TP profile, increases TAWSS local values, especially in the IVC graft region. This results also suggests a beneficial role for IP velocity in reducing the hemodynamic risk of thrombus formation. From the analysis of intravascular flow features emerged that the presence of IP velocity components in the inflow velocity profile imparts a higher level of organization in the blood flowing through the TCPC, not only in the IVC and SVC regions but also in the anastomosis region, ultimately contributing to lower the hydraulic power losses and viscous dissipation rate. This suggest that the establishment of large scale, distinguishable helical flow patterns inside the TCPC could contribute to improve the energetic efficiency of the connection [18] compared to the reference case of one-dimensional only TP velocity profile prescribed as venous inflow BC. These considerations also open the way to rethink how to design the graft and shape the connection, the target the proper shaping of helical flow patterns in the TCPC. There are some main limitations that could weaken the findings of this study: (1) the use of idealized velocity profiles instead of *in-vivo* measured velocity profile, although it was recently demonstrated that the use Womersley profile do not show statistical significant difference in hemodynamics descriptors with respect to the patient-specific three-dimensional velocity profile [9]; (2) the fact that our findings are based on the analysis of only one model.

To conclude, one strong point of the here presented analysis on TCPC hemodynamics it that the applied approach can be easily extended to all those computational hemodynamics studies where fully 3D conditions at boundaries are not available or difficult to measure.

References

[1] P. Khairy, N. Poirier, L.-A. e. Mercier, *"Univentricular Heart"*, Circulation, *115*, 800-812, 2007.

[2] F. Fontan, E. Baudet, *"Surgical reapair of tricuspid atresia"*, Thorax *26*, 8, 1971.

[3] P. D. Coon, J. Rychik, R. T. Novello, P. S. Ro, J. W. Gaynor, T. L. Spray, *"Thrombus formation after the Fontan operation"*, The Annals of Thoracic Surgery, *71*, 5, 2001.

[4] M. Grigioni, C. Daniele, C. Del Gaudio, U. Morbiducci, A. Balducci, G. D'Avenio, A. Amodeo, V. Barbaro, R. Di Donato, *"Numerical simulation of a realistic total cavo-pulmonary connection: Effect of unbalanced pulmonary resistences on hydrodynamic performance"*, Artificial Heart and Cardiac Assist Devices, *26*, 10, 2003.

[5] L. P. Dasi, K. Pekkan, H. Katajima, A. P. Yoganathan, *"Functional Analysis of Fontan Energy Dissipation"*, Journal of Biomechanics, *41*, 13, 2008.

[6] S. Pant, B. Fabrèges, J. F. Gerbeau, I. E. Vignon-Clementel, *"A methodological paradigm for patient-specific multi-scale CFD simulations: from clinical measurements to parameter estimates for individual analysis"*, International Journal for Numerical Methods in Biomedical Engineering, *30*, 1614-1648, 2014.

[7] C. M. Haggerty, M. Restrepo, E. Tang, D. A. de Zélicourt, K. S. Sundareswaran, L. Mirabella, J. Bethel, K. K. Whitehead, M. A. Fogel, A. P. Yoganathan, *"Fontan hemodynamics from 100 patient-specific cardiac magnetic resonance studies: A computational fluid dynamics analysis"*, The Journal of Thoracic and Cardiovascular Surgery, *148*, 1481-1489, 2014.

[8] U. Morbiducci, R. Ponzini, D. Gallo, C. Bignardi, G. Rizzo, *"Inflow boundary conditions for image-based computational hemodynamics: Impact of idealized versus measured velocity profiles in the human aorta"*, Journal of Biomechanics, *46*, 102-109, 2013.

[9] Z. A. Wei, C. Huddleston, P. M. Trusty, S. Singh-Gryzbon, M. A. Fogel, A. Veneziani, A. P. Yoganathan, *"Analysis of Inlet Velocity Profiles in Numerical Assessment of Fontan Hemodynamics"*, Annals of Biomedical Engineering, *47*, 2258-2270, 2019.

[10] K. K. Whitehead, K. Pekkan, H. D. Kitajima, S. M. Paridon, A. P. Yoganathan, M. A. Fogel, *"Nonlinear Power Loss During Exercise in Single-Ventricle Patients After the Fontan: Insights From Computational Fluid Dynamics"*, Circulation, *116*, I-165-I-171, 2007.

[11] F. Migliavacca, G. Dubini, E. L. Bove, M. R. de Leval, *"Computational Fluid Dynamics Simulations in Realistic 3-D Geometries of the Total Cavopulmonary Anastomosis: The Influence of the Inferior Caval Anastomosis"*, Journal of Biomechanical Engineering, *125*, 805-813, 2003.

[12] T. F. Sherman, *"On Connecting Large Vessel to Small"*, Journal of General Physiology, *78*, 23, 1981.

[13] J. R. Womersley, *"Method for the Calculation of Velocity, Rate of Flow and Viscous Drag in Arteries When the Pressure Gradient Is Known"*, Journal of Physiology, *127*, 11, 1955.

[14] L. Zovatto, G. Pedrizzetti, *"Optimal helical entry flow in a helical vessel"*, Fluid Dynamics Research, *50*, 065503, 2018.

[15] W. R. Dean, *"Note on the motion of fluid in a curved pipe"*, The London, Edinburgh, and Dublin Philosophical Magazine and Journal of Science, *4*, 16, 1927.

[16] D. Gallo, D. A. Steinman, P. B. Bijari, U. Morbiducci, *"Helical flow in carotid bifurcation as surrogate marker of exposure to disturbed shear"*, Journal of Biomechanics, *45*, 2398-2404, 2012.

[17] M. Grigioni, G. D'Avenio, A. Amodeo, R. M. Di Donato, *"Power dissipation associated with surgical operations' hemodynamics: Critical issues and application to the total cavopulmonary connection"*, Journal of Biomechanics, *39*, 1583-1594, 2006.

[18] A. Amodeo, M. Grigioni, G. Oppido, C. Daniele, G. D'Avenio, G. Pedrizzetti, S. Giannico, S. Filippelli, R. M. Di Donato, *"The beneficial vortex and best spatial arrangement in total extracardiac cavopulmonary connection"*, The Journal of Thoracic and Cardiovascular Surgery, *124*, 471-478, 2002.